Analysis and Design of Si Terahertz Transit-Time Diodes

Xiaochuan Bi, Jack R. East, Umberto Ravaioli and George I. Haddad

***Abstract*—This paper presents a numerical simulation of a Si MITATT diode working in the submillimeter-wave and lower terahertz frequency range. Both the drift-diffusion model and full band Monte Carlo model are used to investigate the diode DC, small signal and large signal properties. Simulation shows that the Si MITATT diode is not limited by the dead-space of the impact ionization. For the diode under study, the same structure is capable of generating significant RF power at both 200 GHz and 300 GHz.**

***Index Terms*—Transit-Time Diode, Monte Carlo Simulation, Terahertz Frequency**

I. INTRODUCTION

THE terahertz frequency range of the electromagnetic spectrum holds great promise for many applications including sensing, imaging, and communications [1]. However the availability of solid-state power sources with reasonable power levels is well recognized as one of the major obstacles for system applications in this frequency range. Two-terminal devices hold record performance in terms of power generation capability, particularly at higher millimeter- and submillimeter-wave frequencies. They also have the potential of reaching terahertz frequencies and generating significant power levels. Fig. 1 shows the state-of-the-art experimental results of transit-time diodes in cw mode [2, 3].

Most recent work focuses on developing GaAs TUNNETT diodes [3, 4] partially because of the availability of mature material growth technology and quiet noise behavior, but the power is inferior to Si IMPATT diodes [5-7] and inadequate for terahertz system applications. The reasons come from the moderate efficiency of TUNNETT mode operation and material properties. The GaAs figure of merit, $(F_c \times v_{sat})^2$, is half of that of Si, where F_c is the critic field and v_{sat} is the saturation velocity. Wide bandgap materials, GaN and SiC for example, and new device structures have attracted attention to improve the power performance, but they are still limited by present fabrication techniques. In this paper we analyze transit-time diode operation in the terahertz frequency range but focus on the power generation from Si MITATT diodes [8] which have a lower noise measure than IMPATT diodes. Simulation shows that Si MITATT diodes are capable of generating significant power in the terahertz frequency regime.

X. Bi, J. R. East and G. I. Haddad are with the Solid-State Electronics Laboratory, Department of Electrical Engineering and Computer Science, The University of Michigan at Ann Arbor, Ann Arbor, MI 48109-2122 USA (e-mail: xbz@engin.umich.edu; jeast@eecs.umich.edu; gih@eecs.umich.edu).

U. Ravaioli is with the Beckman Institiue and ECE Department, University of Illinois at Urbana-Champaign, Urbana, IL 61801 USA (e-mail: ravaioli@uiuc.edu).

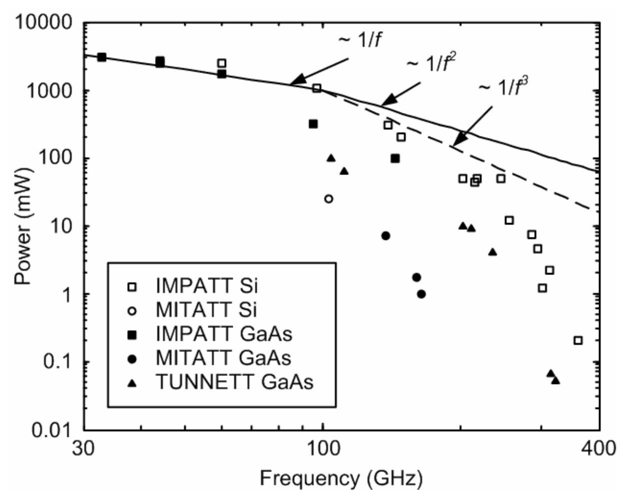

Fig. 1. State-of-the-art RF power levels from transit-time diodes under cw operation in the frequency range from 30 to 400 GHz.

II. SMALL SIGNAL MODEL AND NUMERICAL SIMULATION TECHNIQUE

A. Small signal Model

To operate a Si transit-time diode in the MITATT mode, the generation region electric field needs to be low, normally below 2 MV/cm, to minimize the tunneling [2]. A minimum generation region width is needed to satisfy the breakdown condition $\int \alpha dx = 1$, where α is the ionization coefficient. For the terahertz application, the diode total width is small in order to create a desired drift angle, and therefore the generation region width is relatively large. The Gilden-Hines model for the generation region [9], as shown in Fig. 2(a), assumes a narrow generation region and it is no longer applicable. The Misawa model [10], as shown in Fig. 2(b), should be used instead to account for the transit-time effect in the generation region. The extra negative resistance $-R_g$ comes from the transit time delay in the generation region.

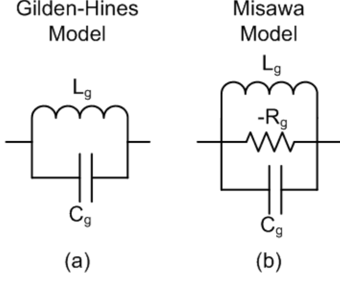

Fig. 2. Equivalent small signal circuit for the generation region.

B. *Drift-Diffusion Model*

The above small signal models explain transit-time diode operation in the linear region. However large signal models are needed to analyze nonlinear effects, design physical structures and estimate RF power generation [11]. The simplest one is the drift-diffusion model which solves the following continuity equations and Poisson's equation numerically,

$$\frac{\partial p}{\partial t} = g - \frac{1}{q}\frac{dJ_p}{dx},$$

$$\frac{\partial n}{\partial t} = g + \frac{1}{q}\frac{dJ_n}{dx},$$

$$\frac{dF}{dx} = \frac{q}{\varepsilon_s}\left[p - n + N_D - N_A\right],$$

where

$$J_p = q\mu_p pF - qD_p \frac{dp}{dx},$$

$$J_n = q\mu_n nF + qD_n \frac{dn}{dx}.$$

The g is the total generation-recombination rate. For the MITATT mode operation where both tunneling and avalanche effects exist, g becomes

$$g = g_a + g_t,$$

where g_a is the avalanche generation rate and g_t is the interband tunneling rate using the Kane's model [12]. The small recombination rate can be ignored.

$$g_a = \frac{1}{q}\left(\alpha_n |J_n| + \alpha_p |J_p|\right),$$

$$g_t = A_T F^2 \exp\left(-B_T / F\right).$$

C. *Monte Carlo Model*

As the frequency approaches the terahertz regime, the carrier transient transport time is comparable to the carrier transit time, and the drift-diffusion model is no longer reliable because of the equilibrium transport assumption. The Monte Carlo (MC) method can be used instead. For low field transport, the electron energy is small and close to the band edge. Therefore the Si bandstructure can be simplified as six equivalent ellipsoidal valleys along the X directions, as shown in Fig. 3. However for high field transport as in the MITATT diode, the electrons distribute in the whole Brillouin zone, and the full bandstructure must be used to describe the density of states and carrier dynamics [13]. The full band MC model used in this paper is described elsewhere [14] which includes the avalanche generation. In addition, the tunneling generation is introduced by adding electrons and holes into the diode according to the tunneling probability using the Kane's model.

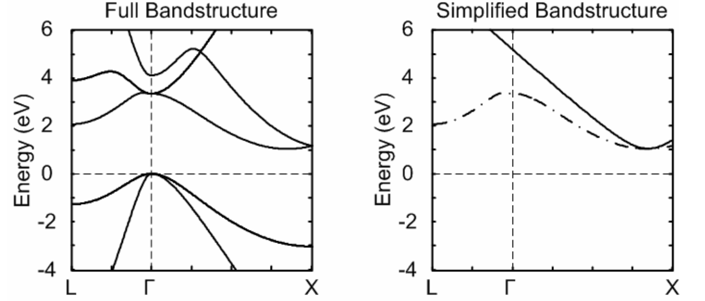

Fig. 3. Si bandstructure. The left one shows the real bandstructure. The right one shows the simplified bandstructure used in a three-valley Monte Carlo program.

D. *Discussion*

The above three models are used in this paper to analyze the Si MITATT diode operation. The drift-diffusion model is used to generate quick numerical solutions and the Misawa model is used to explain the device physics. The full band MC model is more accurate predicting carrier dynamics in the terahertz frequency but requires much longer simulation times. Therefore it is used to confirm the result from the drift-diffusion model. Simulation shows that the drift-diffusion model is useful to predict MITATT diode operation in the terahertz frequency range with proper estimation of generation region width as discussed in section III.

III. MITATT MODE OPERATION

A. *Impact Ionization*

The avalanche process dominates the carrier generation in MITATT mode operation where new carriers are created by the electron and hole impact ionization. In this section the time and space response of the impact ionization is discussed.

Impact ionization is fast, even in the terahertz frequency range, in the sense that the response time for the impact ionization is less than 0.1 ps when driven by a small signal electric field over a DC value of 1 MV/cm, as simulated from the full band MC model. The time for an electron or hole to gain 1 eV of energy is 0.1 about ps if it moves at 10^7 cm/s in a field of 1 MV/cm. Once the carrier accumulates enough energy, it quickly creates a new electron-hole pair due to the large scattering rate for the impact ionization.

But the impact ionization is limited by the dead-space within which the ionization coefficient is zero [15]. The dead-space is associated with the distance required to acquire the initial threshold energy, about one half times of bandgap

energy, to create a new electron-hole pair in order to conserve both energy and momentum. However, later simulation shows that the dead-space only degrades the diode operation by making the generation region wider.

B. DC Results

The drift-diffusion model and full band MC model were used to simulate a Si double drift region (DDR) transit-time diode as shown in Fig. 4. The asymmetric doping profile is used to accommodate the different properties of electrons and holes, yet it is achievable with current growth techniques. To make the comparison more valid, the material parameters used for the drift-diffusion model, the saturation velocities and ionization coefficients, are generated from the full band MC model.

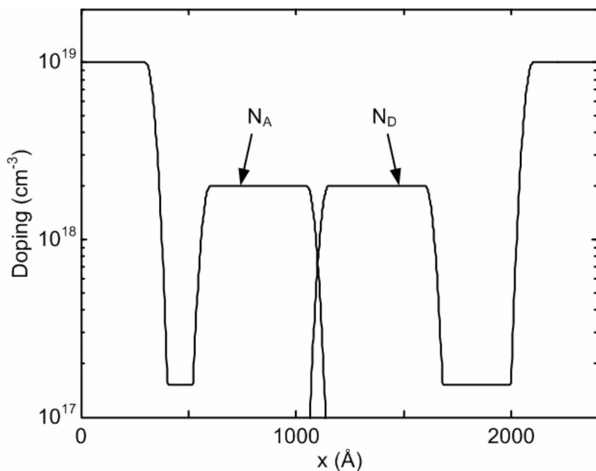

Fig. 4. Si transit-time diode structure.

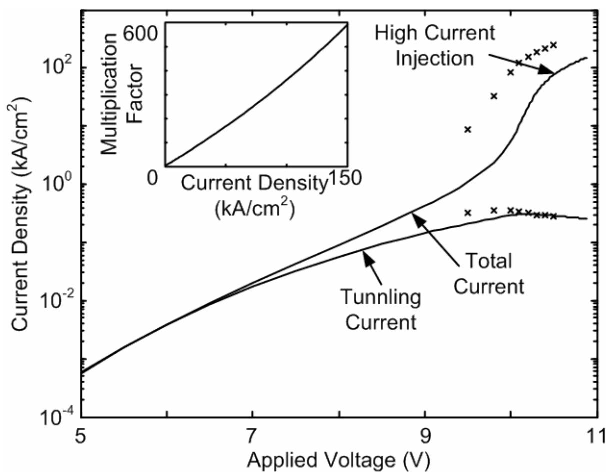

Fig. 5. I-V curve of the diode. The solid lines are from the drift-diffusion model and the x's are from the MC model. The inset shows the multiplication factor as a function of current density from the drift-diffusion model.

Fig. 5 shows the diode DC I-V curves at 500 K. Although the breakdown voltages are slightly different from the two models, both results give similar current curves. The multiplication factor M_a is 600 at a current density of 150 kA/cm^2 and therefore the diode operates in the MITATT mode. The multiplication factor M_a is defined as the total current J_{TOT} divided by the tunneling current J_t, i.e. $M_a \equiv J_{TOT}/J_t$.

An important difference is that the avalanche generation in the MC model are shifted from the central high field generation region towards the outside low field contact regions, resulting in a wider effective generation region, as shown in Fig. 6. This difference comes from the fact that the carriers need space to accumulate energy and release energy. The voltage drop across the shifted space is about the bandgap energy which is the threshold energy needed for impact ionization.

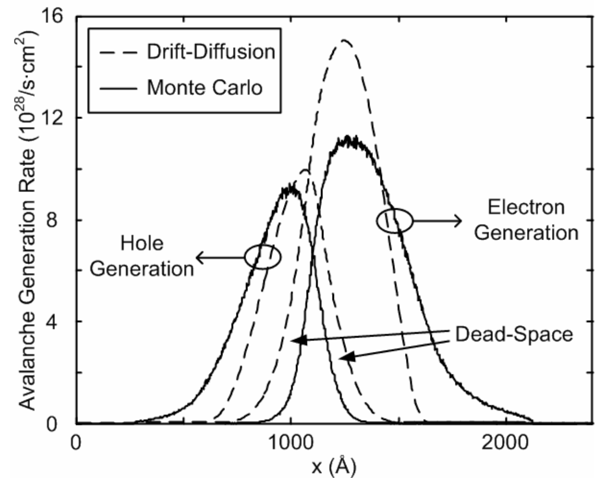

Fig. 6. Avalanche generation rate at current density of 150 kA/cm^2.

C. Small signal Results

The small signal simulation shows a good match between the drift-diffusion model and the full band MC model, as shown in Fig. 7. The reason is that the Si relaxation times are very short compared to the rate of change in the electric field, so the equilibrium transport assumption is still reasonable. One difference is that the avalanche region width is larger from the full band MC model, resulting in smaller negative conductance and larger bandwidth. Nevertheless the drift-diffusion model and hence the Misawa model still give reasonable results.

Although the generation region is not localized, the diode provides negative conductance which comes from the avalanche delay, and the transit-time delay exists both in the drift region and in the generation region. Because the non-localized avalanche region holds the transit-time effect over a wide frequency range, the negative conductance is wideband, as explained from the Misawa model.

The injection current phase angle is shown in Fig. 8. The injection phase angle increases quickly as the avalanche generation starts, and when the current is dominated by the avalanche generation, the injection phase angle is relatively constant. Therefore the power generation from the MITATT

diodes is similar to the IMPATT diodes, as shown in the following large signal results.

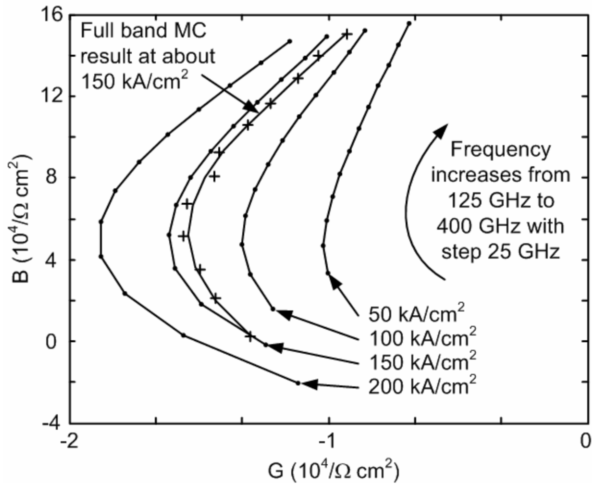

Fig. 7. Diode small-signal admittance G+*i*B.

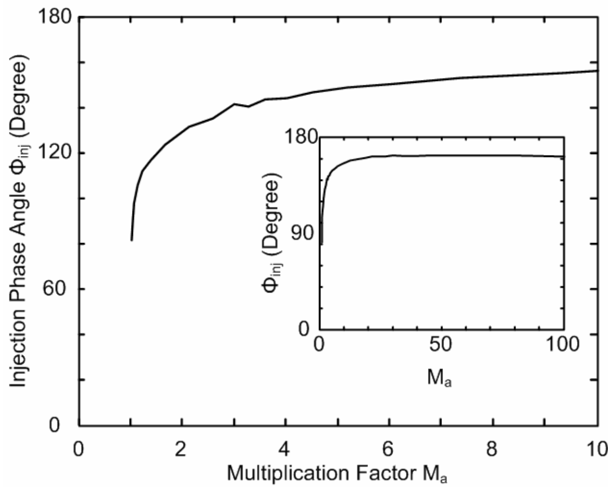

Fig. 8. Injection current phase angle.

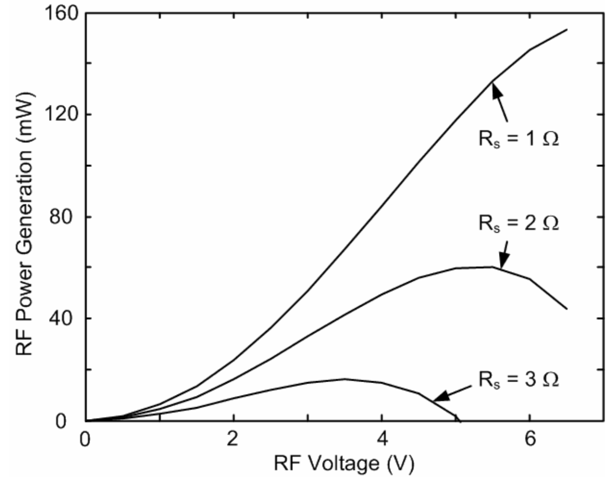

Fig. 9. RF power generation from the Si MITATT diode for different R_s at 200 GHz. J_{DC} = 150 kA/cm^2, r = 6 µm. The contact resistance is 0.9 Ω if the contact resistivity is 10^{-6} Ω·cm^2.

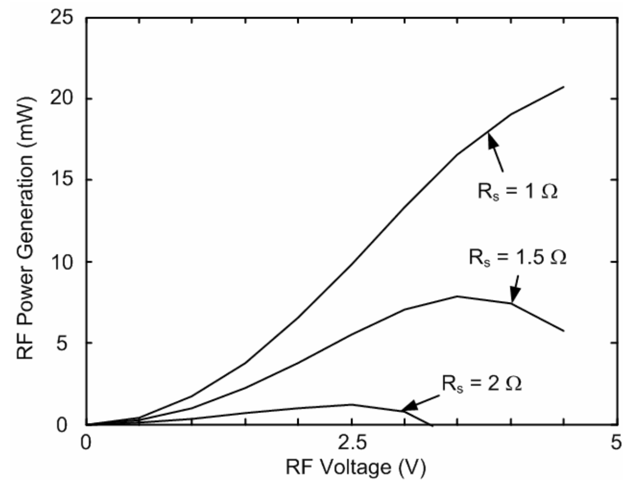

Fig. 10. RF power generation from the Si MITATT diode at 300 GHz. J_{DC} = 175 kA/cm^2, r = 4 µm. The contact resistance is 2 Ω if the contact resistivity is 10^{-6} Ω·cm^2.

D. Large-Signal Results

Because the negative conductance is wideband, the same Si MITATT diode is capable to generate RF power at both 200 GHz and 300 GHz by choosing different device areas, as predicted by the drift-diffusion model. Fig. 9 and Fig. 10 show the power generation for different parasitic losses R_s. The DC current density is increased slightly at 300 GHz in order to increase the negative conductance and therefore RF power generation.

The RF power generation decreases rapidly as R_s increases. Therefore low loss is important. For the transit-time diode, the R_s is dominated by the Ohmic contact resistance and 10^{-6} Ω·cm^2 for the contact resistivity is a conservative number for Si. Much lower resistivity has been reported [16] and even better results can be achieved from a forward biased Schottky contact [17]. Therefore it is possible to reduce the parasitic loss below 1 Ω for both cases.

Although the drift-diffusion model overestimates the RF power generation because the actual avalanche region width is wider and the negative conductance is smaller, the full band MC model shows the diode can still generate significant power at 200 GHz for similar bias condition, as shown in Fig. 11. Actually the power prediction is close to the published Si IMPATT diode data on Fig. 1 at the same frequency range which makes the results reasonable [5-7]. If biased at a higher current density, significant RF power can be expected from 300 GHz as well, as shown in Fig. 12.

IV. CONCLUSION

This paper analyzes Si transit-time devices working in the frequency range from 150 GHz to 400 GHz. Although the drift-diffusion model assumes equilibrium transport, it still gives reasonable results compared with more accurate full band Monte Carlo model. The reason is that the dead-space of

the impact ionization does not limit the Si MITATT diodes operation in this frequency range. It decreases the diodes negative conductance but increases the bandwidth as well. Simulation shows that the Si MITATT diode under study can produce useful power from 200 GHz up to 300 GHz.

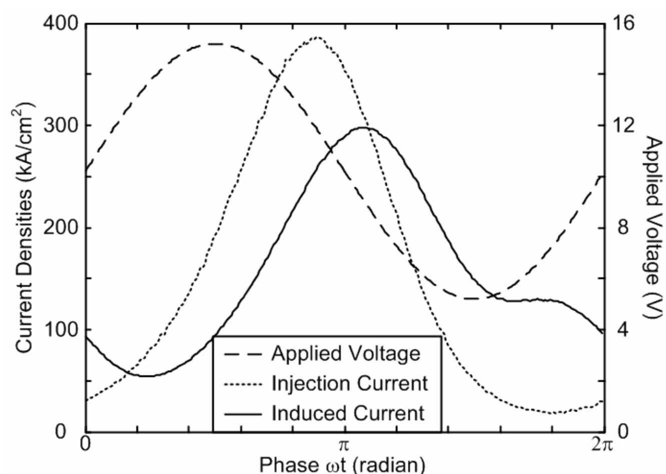

Fig. 11. Large signal operation from the full band MC model at 200 GHz. V_{DC} = 10.2 V, V_{RF} = 5 V, J_{DC} = 157 kA/cm^2, r = 6 µm, R_s = 1 Ω, P_L = 54 mW, η = 3 %.

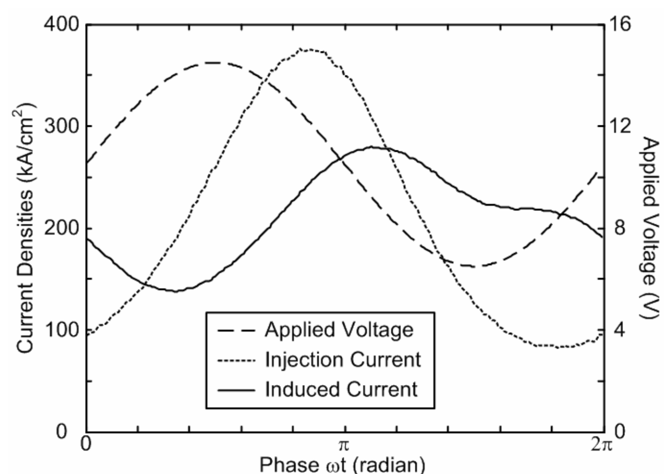

Fig. 12. Large signal operation from the full band MC model at 300 GHz. V_{DC} = 10.5 V, V_{RF} = 4 V, J_{DC} = 211 kA/cm^2, r = 4 µm, R_s = 1 Ω, P_L = 20 mW, η = 1.8 %.

ACKNOWLEDGMENT

This work was supported by ARO under the MURI Program Number DAAD-19-01-1-0622. The authors would like to acknowledge the NSF Network for Computational Nanotechnology for the Monte Carlo codes. The authors would like to thank Dr. Jasprit Singh for helpful discussions.

REFERENCES

[1] Haddad, G.I., J.R. East, and H. Eisele, *Two-Terminal Active Devices for Terahertz Sources*, in *Terahertz Sensing Technology*, M.S. Shur, Editor. 2003, World Scientific.

[2] Eisele, H. and G.I. Haddad, *Active Microwave Diodes*, in *Modern Semiconductor Device Physics*, S.M. Sze, Editor. 1998, John Wiley & Sons, Inc. p. 343-407.

[3] Plotka, P., et al., *240-325-GHz GaAs CW Fundamental-Mode TUNNETT Diodes Fabricated With Molecular Layer Epitaxy.* IEEE Trans. Electron Dev., 2003. **ED-50**(4): p. 867.

[4] Eisele, H., A. Rydberg, and G.I. Haddad, *Recent Advances in the Performance of InP Gunn Devices and GaAs TUNNETT Diodes for the 100-300-GHz Frequency Range and Above.* IEEE Trans. Microwave Theory Tech., 2000. **MTT-48**(4): p. 626.

[5] Chang, K., W.F. Thrower, and G.M. Hayashibara, *Millimeter-Wave Silicon IMPATT Sources and Combiners for the 110-260-GHz Range.* IEEE Trans. Microwave Theory Tech., 1981. **MTT-29**(12): p. 1278.

[6] Chao, C., et al., *Y-Band (170-260 GHz) Tunable CW IMPATT Diode Oscillators.* IEEE Trans. Microwave Theory Tech., 1977. **MTT-25**(12): p. 985.

[7] Ino, M., T. Ishibashi, and M. Ohmori, *C. W. Oscillation with p^+-p-n^+ Silicon IMPATT Diodes in 200 GHz and 300 GHz Bands.* Electron. Lett., 1976. **12**(6): p. 148.

[8] Elta, M.E. and G.I. Haddad, *Mixed Tunneling and Avalanche Mechanisms in p-n Junctions and Their Effects on Microwave Transit-Time Devices.* IEEE Trans. Electron Dev., 1978. **ED-25**(6): p. 694.

[9] Gilden, M. and M.E. Hines, *Electronic Tuning Effects in the Read Microwave Avalanche Diode.* IEEE Trans. Electron Dev., 1966. **ED-13**(1): p. 169.

[10] Misawa, T., *Multiple Uniform Layer Approximation in Analysis of Negative Resistance in p-n Junction in Breakdown.* IEEE Trans. Electron Dev., 1967. **ED-14**(12): p. 795.

[11] Scharfetter, D.L. and H.K. Gummel, *Large-Signal Analysis of A Silicon Read Diode Oscillator.* IEEE Trans. Electron Dev., 1969. **ED-16**(1): p. 64.

[12] Kane, E.O., *Zener Tunneling in Semiconductors.* J. Phys. Chem. Solids, 1959. **12**: p. 181.

[13] Fischetti, M.V. and S.E. Laux, *Monte Carlo Analysis of Electron Transport in Small Semiconductor Devices Including Band-Structure and Space-Charge Effects.* Phys. Rev. B, 1988. **38**(14): p. 9271.

[14] Hess, K., ed. *Monte Carlo Device Simulation: Full Band and Beyond*. The Kluwer International Series in Engineering and Computer Science. 1991, Kluwer Academic Publishers.

[15] Kim, K. and K. Hess, *Simulations of Electron Impact Ionization Rate in GaAs in Nonuniform Electric Fields.* J. Appl. Phys., 1986. **60**(7): p. 2626.

[16] Janega, P.L., J. McCaffrey, and D. Landheer, *Extremely Low Resistivity Erbium Ohmic Contacts to n-Type Silicon.* Appl. Phys. Lett., 1989. **55**(14): p. 1415.

[17] Urteaga, M., et al., *Submicron InP-Based HBTs for Ultra-High Frequency Amplifiers*, in *Terahertz Sensing Technology*, M.S. Shur, Editor. 2003, World Scientific.